Pol. J. Environ. Stud. Vol. XX, No. X (XXXX), 1–9
DOI:*10.15244/pjoes/192980* ONLINE PUBLICATION DATE:

Original research

Coriandrum sativum Mediated Synthesis of Mn_3O_4 Nanoparticles: Structural and Antibacterial Studies

Irum Hanif[1], Misbah Naz[2], Affifa Tajammal[1], Tauqeer Ahmad[3], Shabbir Hussain[4]*, Zeeshan Mustafa[5], Gull Yasmeen[1], Ayesha Kiran[4], Khalid Mashay Al-Anazi[6], Mohammad Abul Farah[6], Amjad Islam[7]

[1]Department of Chemistry, Lahore Garrison University, DHA Phase VI, Lahore, Pakistan
[2]Department of Chemistry, Division of Science and Technology, University of Education Lahore Pakistan
[3]Institute of Chemistry, University of Sargodha, 40100, Pakistan
[4]Institute of Chemistry, Khwaja Fareed University of Engineering and Information Technology, Rahim Yar Khan 64200, Pakistan
[5]Department of Physics, Lahore Garrison University, DHA Phase VI, Lahore, Pakistan
[6]Department of Zoology, College of Science, King Saud University, Riyadh 11451, Saudi Arabia
[7]Key Laboratory for Preparation and Application of Ordered Structured Materials of Guangdong Province, College of Chemistry and Chemical Engineering, Shantou University, Shantou, Guangdong Province, China

Received: 9 April 2024
Accepted: 4 September 2024

Abstract

Mn_3O_4 nanoparticles (NPs) find a broad range of applications in catalysts, energy storage devices, wastewater remediation, biosensors, photocatalysts, medical/antimicrobial agents, and in controlling drug-resistant pathogens. In the present work, Mn_3O_4 NPs were successfully produced by using a simple, cheap, and plant-mediated green synthetic route. The leaf extract of *Coriandrum sativum* was treated with $MnNO_3.6H_2O$ at 60°C and pH 12 to produce Mn_3O_4 NPs. The synthesized NPs were characterized by XRD, FTIR SEM, and UV-Visible analyses. Their electrochemical properties were investigated by cyclic voltammetry (CV) and they were also subjected to antibacterial evaluation studies by the disc diffusion method. The XRD analysis revealed the tetragonal structures of Mn_3O_4 NPs with a crystallite size of 23.62 nm. FTIR spectroscopy displayed the Mn-O vibrations at 730 cm^{-1}. SEM analysis verified the aggregated and flake-like morphology of Mn_3O_4 NPs. UV-Visible spectroscopy revealed the absorption peaks at 232 and 360 nm, which correspond to the permissible charge transfer transitions of $O^{2-} \rightarrow Mn^{2+}$ and $O^{2-} \rightarrow Mn^{3+}$, respectively. The CV curves clearly indicated the redox reactions and the reversible behavior of Mn_3O_4 NPs. The antibacterial activity of Mn_3O_4

*e-mail: shabbir.hussain@kfueit.edu.pk;
shabchem786@gamil.com
Tel.: +92-321-4140130

NPs against *Staphylococcus aureus* (Gram-positive) and *Escherichia coli* (Gram-negative) was also evaluated using ciprofloxacin as a standard reference drug.

Keywords: green synthesis, *Coriandrum sativum*, Mn_3O_4, electrochemical, antibacterial

Introduction

Nanoscale materials are applied across a diverse range of fields including batteries [1, 2], wastewater treatment [3], electronics, magnetics, optoelectronics, biomedicine, pharmaceuticals, cosmetics, energy, environmental science, catalysis, materials science [4], and drug delivery [5]. Manganese oxides e.g., MnO, Mn_5O_8, Mn_2O_3, MnO_2, and Mn_3O_4, have attracted unique attention among the 3d transition metal-oxides due to their diverse structural and chemical variations and find applications in batteries, catalysts, and electrochromic and magnetic materials. Among these, Mn_3O_4 stands out as an effective and affordable catalyst for reducing NO_x and CO emissions, offering a potent method for combating air pollution. Additionally, Mn_3O_4 is being studied as a catalyst for reducing nitrobenzene and oxidizing methane. It has also been found to be a corrosion-inhibiting pigment in epoxy–polyamide and epoxy ester-based primers and topcoats, further highlighting its potential in various industries [6, 7]. Mn_3O_4 (hausmannite) NPs show a broad range of applications in various fields, including catalytic, energy storage devices, wastewater remediation, biosensors, medical, etc. Their bactericidal and photo-catalytic efficiency is significantly affected by their distinct crystalline forms, surface morphologies, synthetic methods, reaction conditions, etc. The fascinating physicochemical properties and distinct structural features of Mn_3O_4 NPs enable them to be used in wastewater treatment and photo-catalytic degradation of dyes under UV and visible light radiations. Their ability to act as antimicrobial agent for the control of drug-resistant microbial populations can be owed to their high reactivity and larger surface-to-volume ratio as compared to bulk materials. The role of Mn_3O_4 NPs in developing epidermal ointments (used for eczema) and for controlling drug-resistant pathogens is well recognized [8]. The fabricated hybrid nanoclusters of OCFC-MnO_2-Mn_3O_4 on oxidized carbon fiber in aqueous 1.0 M Na_2SO_4 electrolyte demonstrated remarkable specific capacitance of 1709 F g^{-1} at 1 A g^{-1} current density [9].

In the past, both chemical and physical routes have been utilized to fabricate uniform-sized NPs with long-term stabilities. However, these methods often involve the use of toxic chemicals, posing negative impacts on human health, so it is important to explore alternative methods to minimize the hazardous effects associated with traditional physical and chemical approaches [10]. Green synthesis of NPs is gaining popularity as a non-toxic, eco-friendly, clean, less expensive, and novel technique [11, 12]. The environmentally friendly synthesis of NPs with regular form and size, using genetic engineering techniques, molecular cloning, plant extracts, and other biological methods, represents a significant advancement in nanobiotechnology [13, 14]. Plants, fungi, bacteria, yeasts, algae, and actinomycetes may all be used to produce biogenic-metallic NPs, which alters the metal's characteristics significantly [15]. The growing interest in efficient green chemistry has led to a focus on plant-mediated synthesis of nanoparticles. Plant extracts can reduce and stabilize metal nanoparticles in a single-step synthesis, leveraging their natural characteristics. A variety of natural organic compounds in plant extracts, such as alkaloids, flavonoids, saponins, steroids, terpenoids, and tannins, serve as both reducing and stabilizing agents [16]. Plants are also rich in phenolics and flavonoids, which act as powerful antioxidants [17, 18].

The *Coriandrum Sativum* (an annual herb) belongs to Apiaceae (Umbelliferae) family and is also known by the names of Chinese parsley, coriander, dhania, cilantro, etc. [19]. It is commonly grown in India, Italy, the Netherlands, Central and Eastern Europe, China, and Bangladesh. Different portions of *C. sativum* have the ability to yield essential oil, flavonoids, fatty acids, and sterols [20]. Green coriander consists of 84% water; essential oils and fatty oil are its active ingredients. The essential oil content of ripened and dried coriander ranges from 0.03 to 2.6 percent, with fatty oil content ranging from 9.9 to 27.7%; the major component of essential oil is S-(+)-linalool (60–70%) with the existence of monoterpene hydrocarbons as minor active ingredients [21].

Recent studies are focused on the plant-mediated synthesis of Mn_3O_4 NPs using *Coriandrum sativum* leaf extract. The biosynthesized NPs were characterized by XRD, FT-IR, SEM, and UV/VIS spectroscopy and also evaluated for their electrochemical and antimicrobial potential.

Materials and Methods

Coriandum Sativum powder, de-ionized water**,** manganese (II) nitrate hexahydrate (analytical grade)**,** methanol (Analytical grade), and 0.1 N solution of NaOH were used for the green synthesis.

The synthesized NPs' phase nature and crystallinity were analyzed using an X-Ray Diffractometer. FT-IR spectroscopy was performed in the range of 500–4000 cm^{-1} using a Carry 630 model. SEM analysis was performed by the JEOL JSM-6480LV model. UV-Visible spectroscopy was performed by a UV-3002 spectrometer in the range of 200

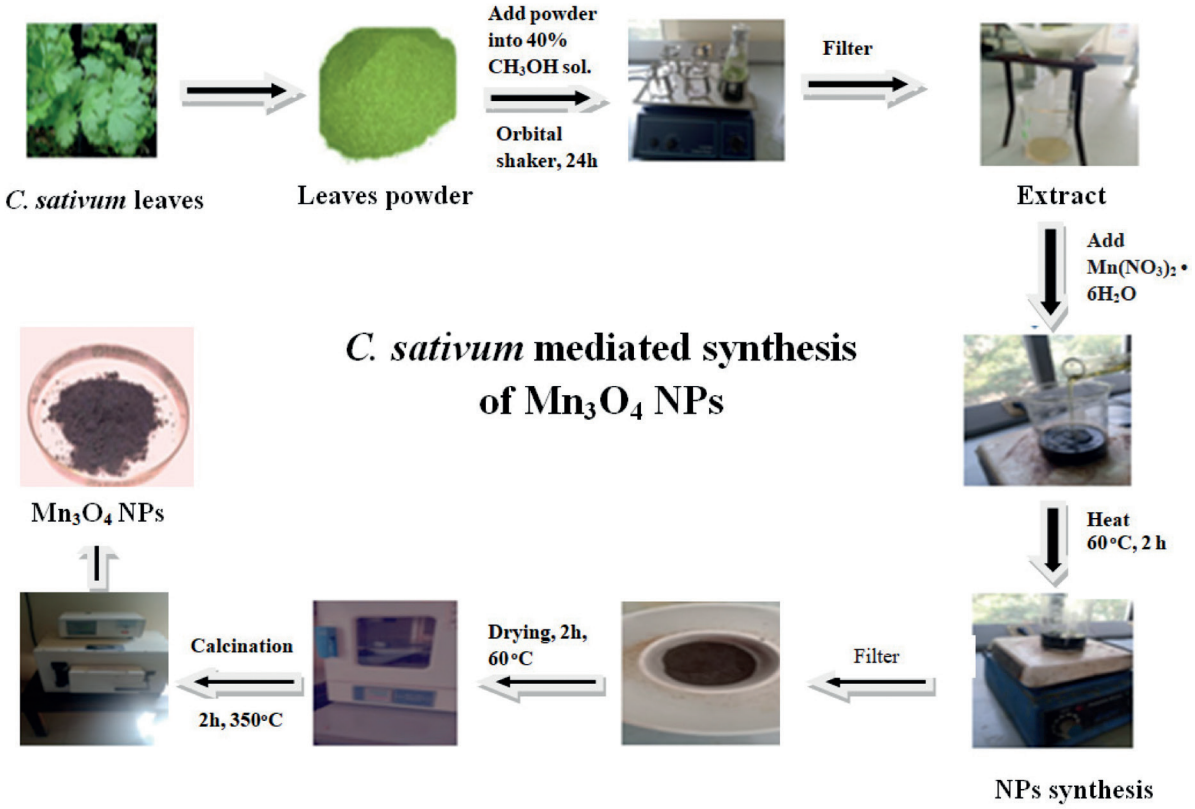

Fig. 1. *C. sativum* mediated synthesis of Mn_3O_4 NPs.

to 900 nm. The electrochemical behavior of the synthesized NPs was investigated using a Galvanostat/Potentiostat of the CS300 model. Cyclic voltammetry was performed by using a reported procedure [22].

Antibacterial activities were performed at the Department of Biochemistry, University of Agriculture, Faisalabad, Pakistan by using the disc diffusion method. The samples were tested against *Staphylococcus aureus* (Gram-positive) and *Escherichia coli* ATCC 25922 (Gram-negative). The Institute of Microbiology at the University of Agriculture, Faisalabad, Pakistan, confirmed the purity and identity of the product. Nutrient agar was used as the growth medium. The inhibition zones were recorded in millimeters by a zone reader [23].

Collection and Powdering of Plant Material

The leaves of *Coriandrum sativum* (Fig. 1) plant were purchased from Ichra Market of Lahore (Punjab), Pakistan in August 2021. The plant species was verified by the Department of Biology, Lahore Garrison University Lahore, Pakistan.

The *C. Sativum* leaves were cleaned with fresh water and then with distilled water to remove dirt and contaminants. They were dried at room temperature for 24 hours to eliminate the moisture. The dried leaves were ground in a steel grinder to obtain a homogenized powder, which was then sieved to a mesh size of 100 µm.

Preparation of Extract

30 g of *C. sativum* leaves powder was soaked in 100 mL of 40% methanol. The solution was stirred for 24 hours at ambient temperature. It was then filtered, and the filtrate was centrifuged to remove any residual impurities, and refrigerated at 4°C for usage within a week.

Synthesis of Manganese NPs

30 mL of 5% manganese (II) nitrate hexahydrate solution in water was taken in a 250 mL beaker. 30 mL of *C. sativum* leaves extract was added to it, and the pH of the solution was adjusted to 12 by adding NaOH solution (0.1 N) dropwise. The solution was stirred for 2 hours at 60ºC, then cooled and centrifuged at 2000 rpm for 15 min at ambient temperature. The color of the solution changed from dark green to light green, confirming the bio-synthesis of Mn_3O_4 NPs. The solution was finally filtered to separate the precipitated Mn_3O_4 NPs (1.75 g). After drying, the NPs were ground into powder and added to a China dish which was finally placed in a muffle furnace at 350ºC for 2 hours for calcination to leave behind the dried green crystals of Mn_3O_4 NPs (0.65 g).

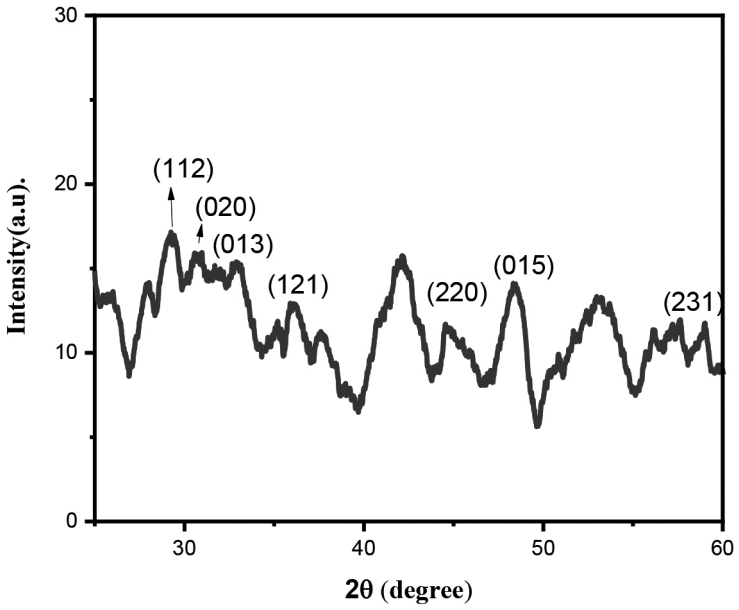

Fig. 2. XRD spectrum of Mn_3O_4 NPs.

Results and Discussion

C. sativum leaves powder (30 g) was soaked in 40% methanol (100 mL), stirred for 24 hours, filtered, and centrifuged to leave behind the clear extract of the plant. Then, manganese (II) nitrate hexahydrate solution (5%) was mixed with *C. sativum* extract (30 mL) and pH was adjusted to 12 by adding NaOH followed by stirring at 60°C for 2 hours, cooling and centrifugation to separate out the green-colored precipitates of Mn_3O_4 NPs which were calcined at 350ºC to leave behind the final product. The applied synthetic method uses the leaf extract of *C. sativum* as a reducing and stabilizing agent for the synthesis of Mn_3O_4 NPs. The synthesized NPs were subjected to XRD, FTIR, SEM, and UV-visible analyses. They were also tested for electrochemical potential by cyclic voltammetry and their antibacterial activity was also evaluated by the disc diffusion method.

XRD Analysis

The XRD pattern (Fig. 2) exhibited prominent diffraction peaks at 2θ values of 29.38°, 30.91°, 33.01°, 36.13°, 38.19°, 44.80°, 49.6°, and 58.99°, corresponding to the Miller indices 112, 020, 013, 121, 022, 220, 015, and 231, respectively. These peaks are consistent with the JCPDS CARD number 03-065-2776, indicating the tetragonal crystal structure characteristic of Mn_3O_4 [24]. The crystallite sizes of Mn_3O_4 NPs were calculated by applying the Debye–Scherer Equation 1 [25].

$$D = \frac{k\lambda}{\beta\cos\theta} \quad (1)$$

Where K = 0.94, which depends on the shape of crystallites, β represents the peak's highest width at half maximum, λ is the wavelength (0.154), D is particle size, and θ is diffraction angle. Using the Debye-Scherer equation, the average grain size of Mn_3O_4 NPs was found to be 23.62 nm.

FT-IR Spectroscopy

FT-IR spectrum of synthesized NPs was recorded in the range of 4000 to 500 cm^{-1} and is shown in Fig. S1 (Supplementary Material). A peak at 3650 cm^{-1} indicates the presence of the -OH group of H_2O [26]. The broad band at 2935 cm^{-1} shows the presence of the CH_2 stretching vibrations of the coriander leaves [27]. A shift in the peak of the C=O group from 1624 cm^{-1} to 1708 cm^{-1} is attributed to the formation of Mn_3O_4 NPs. Three peaks ranging from 1574 to 1515 cm^{-1} represent the C=C group. The broad band at 1160 cm^{-1} shows the presence of the C–N vibrations whereas the band at 1026 cm^{-1} is associated with the stretching vibration of the C–O–C or C–O groups that, together with C=C groups, are related to phytochemicals which are present in the plant as flavones, alkaloids, phenols, and anthracenes that can help to generate metallic nanoparticles according to the literature [28]. A peak at 1557 cm^{-1} shows the C–H bending vibration [29]. The bending of the adsorbed OH vibration combined with Mn NPs occurs at 1393 cm^{-1} [30]. The 730 cm^{-1} peak indicates the MnO stretching in tetrahedral and octahedral sites [29].

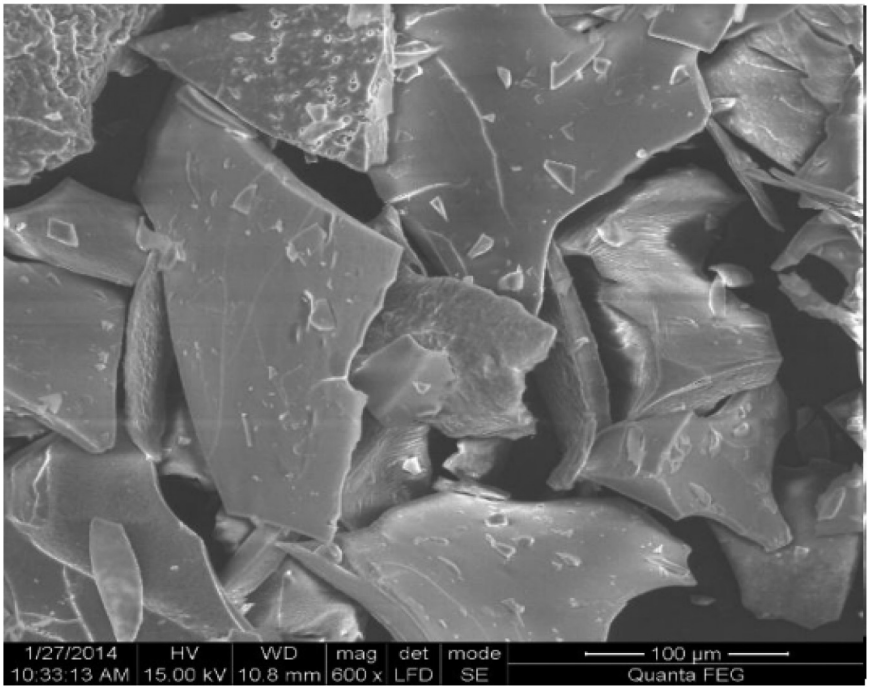

Fig. 3. SEM image of Mn_3O_4 NPs.

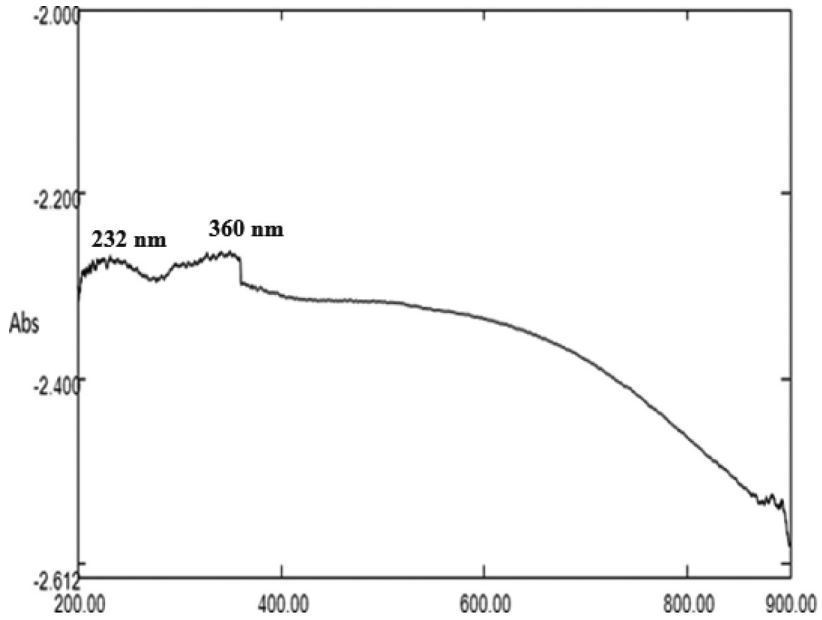

Fig. 4. UV-Visible spectrum of Mn_3O_4 NPs.

SEM Analysis

The surface structure and size of the Mn_3O_4 NPs were examined using Scanning Electron Microscopy (SEM); the obtained image is shown in Fig. 3. The surface morphology of the Mn_3O_4 NPs appeared agglomerated. The aggregated form of Mn_3O_4 NPs also exhibited a flake-like structure [31]. The particle size of Mn_3O_4 NPs was 34.17 nm.

UV-Visible Spectroscopy

The absorption peaks were observed at 232 nm and 360 nm in UV-Visible absorption spectrum of Mn_3O_4 (Fig. 4) and correspond to the permissible charge transfer transitions of $O^{2-} \rightarrow Mn^{2+}$ and $O^{2-} \rightarrow Mn^{3+}$, respectively [32].

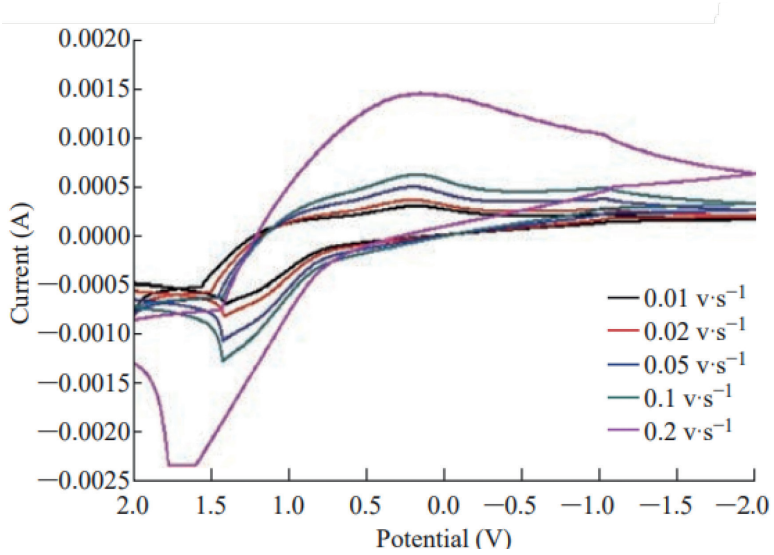

Fig. 5. CV curves of Mn_3O_4 NPs.

Table 1. Calculation of redox current and redox potential of Mn_3O_4 NPs.

Scan rate mV/s	Anodic Potential (Va)	Cathodic Potential (Vc)	Total Redox Potential	Anodic Current (Ia)	Cathodic Current (Ic)	Total Redox Current
0.01	0.100	6.857	65.870	2.180	-7.998	-79.980
0.02	0.141	9.096	64.512	19.360	-9.500	-67.532
0.05	0.223	9.751	43.74	16.950	-12.260	-55.364

Cyclic Voltammetry (CV)

The CV curves of Mn_3O_4 NPs at various scan speeds are shown in Fig. 5, together with data on the transfer of electrons, kinematics, and transportation characteristics of the electrolytic reaction. The current flow was measured relative to the supplied linear voltage. The processes that take place at the surface of the electrode can be better understood by examining the current fluctuation that results from the different electrode potentials.

Cyclic voltammetry (CV) was employed to assess the electrochemical behavior of Mn_3O_4 NPs in redox reactions at an electrode in distilled water, using scanning speeds ranging from 0.01 to 0.2 V/s and a voltage range of 2 to -2 V. At a scanning rate (υ) of 0.1 V/s, two oxidation peaks were observed for Mn^{2+} to Mn^{3+} and Mn^{3+} to Mn^{4+} transitions. The oxidation peaks were detected at Epox1 = -0.735 V and Epox2 = -1.050 V, with corresponding anodic peak currents Ipox1 = 1.6×10^{-4} and Ipox2 = 4.868×10^{-4}, respectively. A single reduction peak was observed at Ep_{red} = -0.526 V, corresponding to an anodic current maximum Ip_{red} = -1.05×10^{-4} A. The voltammetry results of an electrode containing Mn_3O_4 NPs in the presence of 1 ppm $MnSO_4$ solution at different scanning rates (0.01, 0.02, and 0.05 V/s) are presented in Table 1.

Antibacterial Activity

NPs were evaluated for their antibacterial potential against *Escherichia coli* (G-negative) and *Staphylococcus aureus* (G-positive) by the disc diffusion method. Ciprofloxacin was used as a positive control, while discs containing only water were employed as a negative control. A zone reader was used to measure zones of inhibition in mm. The zones of inhibition (ZOI) of Mn_3O_4 NPs were found to be 12 mm and 3 mm against *E. coli* and *S. aureus*, respectively; the observed activities were significantly smaller as compared to 37 mm and 40 mm zones of ciprofloxacin against *E. coli* and *S. aureus*, respectively.

Conclusions

A simple, environmentally sound, cheap, and novel green approach was employed for the synthesis of Mn_3O_4 NPs from *Coriandrum sativum* extract. The characterization

of the NPs was performed by XRD, FTIR SEM, and UV-Visible analyses. X-ray diffraction (XRD) studies revealed the tetragonal configuration with a crystallite size of 23.62 nm. FTIR vibrations at 730 cm^{-1} were attributed to the Mn-O stretching mode. There was involvement of alcohol and ethers in the reduction of metal ions and capping of formed NPs. SEM analysis confirmed the aggregated and flake-like structures of Mn_3O_4 NPs with a particle size of 34.17 nm. UV-Visible spectroscopy has shown the absorption peaks at 232 and 360 nm, which correspond to correspond to the permissible charge transfer transitions of $O^{2-} \rightarrow Mn^{2+}$ and $O^{2-} \rightarrow Mn^{3+}$, respectively. Cyclic voltammetry has verified the redox nature and reversible behavior of synthesized material. The synthesized NPs were tested for their antibacterial activities by disc diffusion method using the standard drug ciprofloxacin and have shown some antimicrobial potential against *E. coli* and *S. aureus*.

Acknowledgments

The authors would like to extend their sincere appreciation to the Researchers Supporting Project number (RSP2024R154), King Saud University, Riyadh, Saudi Arabia.

Conflict of Interest

The authors declare that there is no conflict of interest between the authors.

References

1. ABBAS S.M., HUSSAIN S.T., ALI S., MUNAWAR K.S., AHMAD N., ALI N. Facile synthesis of carbon nanotubes supported NiO nanocomposite and its high performance as lithium-ion battery anode. Materials Letters. **107**, 158, **2013**.
2. IQBAL M., MUNEER M., RAZA R., SALEEM M., HUSSAIN S., REHMAN Z.U., ABBAS F., ALI S., JAVED M.A., HUSSAIN M. Recycling of lead from lead acid battery to form composite material as an anode for low temperature solid oxide fuel cell. Materials Today Energy. **16**, 100418, **2020**.
3. REHMAN H., ALI Z., HUSSAIN M., GILANI S., SHAHZADY T., ZAHRA A., HUSSAIN S., HUSSAIN H., HUSSAIN I., FAROOQ M. Synthesis and characterization of ZnO nanoparticles and their use as an adsorbent for the arsenic removal from drinking water. Digest Journal of Nanomaterials and Biostructures. **14** (4), 1033, **2019**.
4. BISWAS P., WU C.-Y. Nanoparticles and the environment. Journal of the Air & Waste Management Association. **55** (6), 708, **2005**.
5. ZULFIQAR H. Nature of nanoparticles and their applications in targeted drug delivery. Pakistan Journal of Science. **72** (1), 30, **2020**.
6. WEIXIN Z., CHENG W., XIAOMING Z., YI X., YITAI Q. Low temperature synthesis of nanocrystalline Mn3O4 by a solvothermal method. Solid State Ionics. **117** (3–4), 331, **1999**.
7. VÁZQUEZ-OLMOS A., REDÓN R., RODRÍGUEZ-GATTORNO G., MATA-ZAMORA M.E., MORALES-LEAL F., FERNÁNDEZ-OSORIO A.L., SANIGER J.M. One-step synthesis of Mn3O4 nanoparticles: Structural and magnetic study. Journal of Colloid and Interface Science. **291** (1), 175, **2005**.
8. SUKHDEV A., CHALLA M., NARAYANI L., MANJUNATHA A.S., DEEPTHI P., ANGADI J.V., KUMAR P.M., PASHA M. Synthesis, phase transformation, and morphology of hausmannite Mn3O4 nanoparticles: photocatalytic and antibacterial investigations. Heliyon. **6** (1), **2020**.
9. SUN X., WANG J., CHEN B., DAI G., SITU Y., HUANG H. High-performance adjustable manganese oxides hybrid nanostructure for supercapacitors. Electrochimica Acta. **381**, 138213, **2021**.
10. HUSSAIN S., AZIZ I., WAQAS M., AHMAD T., AHMAD I., TAHIR M.B., AL HUWAYZ M., ALWADAI N., IQBAL M., NAZIR A. Potential Antifungal and Antimicrobial Effects of Nano Zinc Oxide Particles Obtained from Cymbogobon citratus Leaf Extract Using Green Technology. Polish Journal of Environmental Studies. **32** (5), 4065, **2023**.
11. HUSSAIN S., ALI MUAZZAM M., AHMED M., AHMAD M., MUSTAFA Z., MURTAZA S., ALI J., IBRAR M., SHAHID M., IMRAN M. Green synthesis of nickel oxide nanoparticles using Acacia nilotica leaf extracts and investigation of their electrochemical and biological properties. Journal of Taibah University for Science. **17** (1), 2170162, **2023**.
12. RIAZ T., ASGHAR A., SHAHZADI T., SHAHID S., MANSOOR S., ASGHAR A., JAVED M., IQBAL S., ALOTAIBI M.T., ALTHOBITI R.A. Green synthesis of ZnO and Co-ZnO using Brassica rapa leave's extract and their activities as antioxidant agents, efficient adsorbents, and dye removal agents. Journal of Saudi Chemical Society. **27** (5), 101716, **2023**.
13. ZHAN Q., HAN J., SHENG L. Iron nanoparticles green-formulated by Coriandrum sativum leaf aqueous extract: investigation of its anti-liver-cancer effects. Archives of Medical Science. **2022**.
14. JAVED M., HUSSAIN S., RIAZ M., ASGHAR A., SYED S., BARKAAT S., SULEMAN M., IDREES M., ASHRAF F., FAIZAN M. Synthesis and characterization of nanoparticles derived from chitosan-based biopolymer; their photocatalytic and anti-termite potential. Digest Journal of Nanomaterials & Biostructures. **16** (4), 1607, **2021**.
15. GNANAJOBITHA G., ANNADURAI G., KANNAN C. Green synthesis of silver nanoparticle using Elettaria cardamomom and assesment of its antimicrobial activity. International Journal of Pharmaceutical Sciences and Research. **3** (3), 323, **2012**.
16. ISHAK N.M., KAMARUDIN S., TIMMIATI S. Green synthesis of metal and metal oxide nanoparticles via plant extracts: an overview. Materials Research Express. **6** (11), 112004, **2019**.
17. FARHAT N., HUSSAIN S., SYED S.K., AMJAD M., JAVED M., IQBAL M., HUSSAIN M., HAROON S.M., RAZA H., BUTT S.Z. Dietary phenolic compounds in plants: Their antioxidant and pharmacological potential. Postepy Biologii Komorki. **47** (3), 307, **2020**.
18. REHMAN A., HUSSAIN S., JAVED M., ALI Z., REHMAN H., SHAHZADY T.G., ZAHRA A. Chemical composition and remedial perspectives of Hippophae rhamnoides linn. Postepy Biologii Komorki. **45** (3), 199, **2018**.

19. MANJUNATHA R., USHARANI K., NAIK D. Synthesis and characterization of ZnO nanoparticles: A review. Journal of Pharmacognosy and Phytochemistry. **8** (3), 1095, **2019**.
20. JAHAN I., ERCI F., ISILDAK I. Facile microwave-mediated green synthesis of non-toxic copper nanoparticles using Citrus sinensis aqueous fruit extract and their antibacterial potentials. Journal of Drug Delivery Science and Technology. **61**, 102172, **2021**.
21. PATHAK N.L., KASTURE S.B., BHATT N.M., RATHOD J.D. Phytopharmacological properties of Coriander sativum as a potential medicinal tree: an overview. Journal of Applied Pharmaceutical Science, **1** (4), 20, **2011**.
22. YASMEEN G., HUSSAIN S., TAJAMMAL A., MUSTAFA Z., SAGIR M., SHAHID M., IBRAR M., ELQAHTANI Z.M., IQBAL M. Green Synthesis of Cr2O3 Nanoparticles by Cassia Fistula, their Electrochemical and Antibacterial Potential. Arabian Journal of Chemistry. **16**, 104912, **2023**.
23. MUZAFFAR J., METCALFE C., COLLEY S., COULSON C. Diffusion-weighted magnetic resonance imaging for residual and recurrent cholesteatoma: a systematic review and meta-analysis. Clinical Otolaryngology. **42** (3), 536, **2017**.
24. JAMIL S., KHAN S.R., SULTANA B., HASHMI M., HAROON M., JANJUA M.R.S.A. Synthesis of saucer shaped manganese oxide nanoparticles by co-precipitation method and the application as fuel additive. Journal of Cluster Science. **29**, 1099, **2018**.
25. FATHIMA J.B., PUGAZHENDHI A., OVES M., VENIS R. Synthesis of eco-friendly copper nanoparticles for augmentation of catalytic degradation of organic dyes. Journal of Molecular Liquids. **260**, 1, **2018**.
26. SALGUERO SALAS M.A. Síntesis y caracterización de nanopartículas de plata usando como reductores extractos de menta (Origanum vulgare) y cilantro (Coriandrum sativum), y como funcionalizante el látex de sangre de drago (Croton lechleri). Thesis, Pontificia Universidad Católica del Ecuador. **2016** [In Spanish].
27. ACHARYA G.C., PONNAM N., KUMARI M., ROY T.K., SHIVASHANKARA K.S., SAHOO M.R. Phytochemical profiling of spiny coriander (Eryngium foetidum L.)–A potential perennial spicing-culinary herb of eastern India. Acta Chromatographica. **34** (2), 197, **2021**.
28. SINGH J., DUTTA T., KIM K.-H., RAWAT M., SAMDDAR P., KUMAR P. Green'synthesis of metals and their oxide nanoparticles: applications for environmental remediation. Journal of Nanobiotechnology. **16**, 1, **2018**.
29. AHMED K.A.M., HUANG K. Formation of Mn3O4 nanobelts through the solvothermal process and their photocatalytic property. Arabian Journal of Chemistry. **12** (3), 429, **2019**.
30. VERSIANI A.F., ANDRADE L.M., MARTINS E.M., SCALZO S., GERALDO J.M., CHAVES C.R., FERREIRA D.C., LADEIRA M., GUATIMOSIM S., LADEIRA L.O. Gold nanoparticles and their applications in biomedicine. Future Virology. **11** (4), 293, **2016**.
31. SHAIK M.R., SYED R., ADIL S.F., KUNIYIL M., KHAN M., ALQAHTANI M.S., SHAIK J.P., SIDDIQUI M.R.H., AL-WARTHAN A., SHARAF M.A. Mn3O4 nanoparticles: Synthesis, characterization and their antimicrobial and anticancer activity against A549 and MCF-7 cell lines. Saudi Journal of Biological Sciences. **28** (2), 1196, **2021**.
32. MACSTRE J.B., LÓPEZ E.F., GALLARDO-AMORES J., CASERO R.R., ESCRIBANO V.S., BERNAL E.P. Influence of tile synthesis parameters on the structural and textural properties of precipitated manganese oxides. International Journal of Inorganic Materials. **3** (7), 889, **2001**.

Supplementary Material

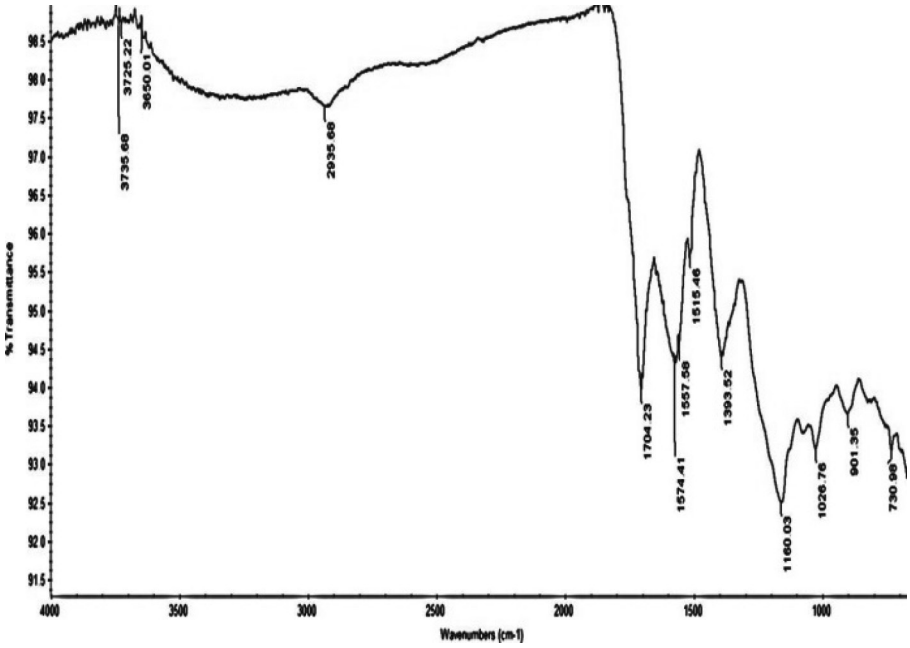

Fig. S1. FTIR spectrum of Mn_3O_4 NPs.